TALLINN UNIVERSITY OF TECHNOLOGY

SCHOOL OF ENGINEERING

DEPARTMENT OF MATERIALS SCIENCE

Temperature-dependent optoelectrical characterization of $Cu_2CdGeSe_4$-based Monograin Layer Solar Cells

$Cu_2CdGeSe_4$-l baseeruvate monoterakihiliste päikesepatareide temperatuurist sõltuv optoelektriline iseloomustamine

Master Thesis

Student: Robert Beglaryan

Student Code: 184580KAYM

Supervisor: Mati Danilson, Researcher

Tallinn 2020

AUTHOR'S DECLARATION

Hereby I declare, that I have written this thesis independently.

No academic degree has been applied for based on this material. All works, major viewpoints and data of the other authors used in this thesis have been referenced.

".....” ..... 20…..

Author: Robert Beglaryan .....

/signature /

The thesis is in accordance with terms and requirements

".....” ..... 20….

Supervisor: Mati Danilson .....

/signature/

Accepted for defence

".....”.....20… .

Chairman of theses defence commission: .....

/name and signature/

DEPARTMENT OF MATERIALS SCIENCE

THESIS TASK

Student: Robert Beglaryan, 184580KAYM

Study programme: KAYM09/18 - Materials and Processes for Sustainable Energetics

Main speciality: Materials for sustainable energetics

Supervisor: Mati Danilson, researcher, +3725537477

Thesis topic: *Temperature-dependent optoelectrical characterization of Cu2CdGeSe4-based Monograin Layer Solar Cells / Cu2CdGeSe4-l baseeruvate monoterakihiliste päikesepatareide temperatuurist sõltuv optoelektriline iseloomustamine*

Thesis main objectives:

1. Obtain temperature-dependent current-voltage characteristics and measure external quantum efficiency for studied solar cells

2. Analyze the results, estimate the diode circuit parameters and parasitic loss parameters and study their dependences on temperature and light intensity

3. Compare the results for the devices with different preparation, understand how did the difference in the preparation affect the device performance

Thesis tasks and time schedule:

No	Task description	Deadline
1.	Literature review	01.02.19
2.	Experimental part – IV and EQE measurements	01.03.20
3.	Analysis of results, conclusions	10.04.20

Language: English, **Deadline for submission of thesis: "....."..... 2020**

Student: Robert Beglaryan **..... *[signature]* "....."..... 2020**

Supervisor: Mati Danilson **..... *[signature]* "....."..... 2020**

Head of study programme: Sergei Bereznev **..... *[signature]* "....."..... 2020**

Table of Contents

Preface

The following work has been made in frames of the program “Materials and Processes of Sustainable Energetics” at Tallinn University of Technology. The main work and experiments have been done in the Laboratory of Optoelectronic materials physics, under the supervision of researcher Mati Danilson.

My studies and execution of the project were made possible by the generous funding of the Estonian Ministry of Foreign Affairs, to which I am grateful. I am also grateful to Mati Danilson for the support and very thoughtful supervision of my work, dr. Marit Kauk-Kuusik for providing the samples studied in this work and useful insights, and my colleagues in the lab who were always ready to give me advice and guidance when needed.

This work was supported by institutional research funding IUT19-28 of the Estonian Ministry of Education and by the European Union through the European Regional Development Fund project TK141 “Advanced materials and high-technology devices for sustainable energetics, sensorics and nanoelectronics” I would like to say a special thank you to my family, who were always supporting me even in the most challenging times.

In this project, temperature-dependent current-voltage (J-V) characteristics and external quantum efficiency (EQE) of CCGSe-based MGL solar cells with differences in preparation were studied. The work is aimed to find the diode circuit parameters (ideality factor and dark saturation current) and parasitic loss parameters (series resistance and parallel resistance) from J-V curves and study their dependences on temperature and light intensity. Based on the results, we can conclude if the different treatment method improved the performance of the solar cell.

Keywords: Master’s Thesis, Solar Cells, Current-Voltage measurements, External Quantum efficiency measurement, $Cu_2CdGeSe_4$

List of abbreviations, acronyms, and symbols

- ktoe - kiloton of oil equivalent
- PV - photovoltaic(s)
- GWh - Giga Watt-hour
- MGL - monograin layer
- CCGSe - $Cu_2CdGeSe_4$
- CIGS - $CuInGaSe_2$
- CdTe - Cadmium telluride
- CdS - Cadmium sulfide
- QE - quantum efficiency
- EQE - external quantum efficiency
- IQE - internal quantum efficiency
- eV - electron volt
- E_g - band gap energy
- J_{ph} - photo-generation current density
- V_{oc} - open-circuit voltage
- V_{mp} - maximum power-point voltage
- J_{sc} – short-circuit current
- J_{mp} - maximum power-point current density
- FF - fill factor
- A_c - area of the cell
- R_s - series resistance
- R_p – parallel (shunt) resistance

Chapter 1 – Introduction

1.1 Background

One of the most important and challenging issues of modern energy production and usage is the tremendous dependence on non-renewable energy sources. As can be seen in figure 1.1, the integral part of energy production is based on depleting energy sources. Under the assumption that the population of mankind does not change drastically, and it consumes energy at the current level, the fossil fuel reserves will be exhausted within 320 years and the nuclear energy within 260 years [1].

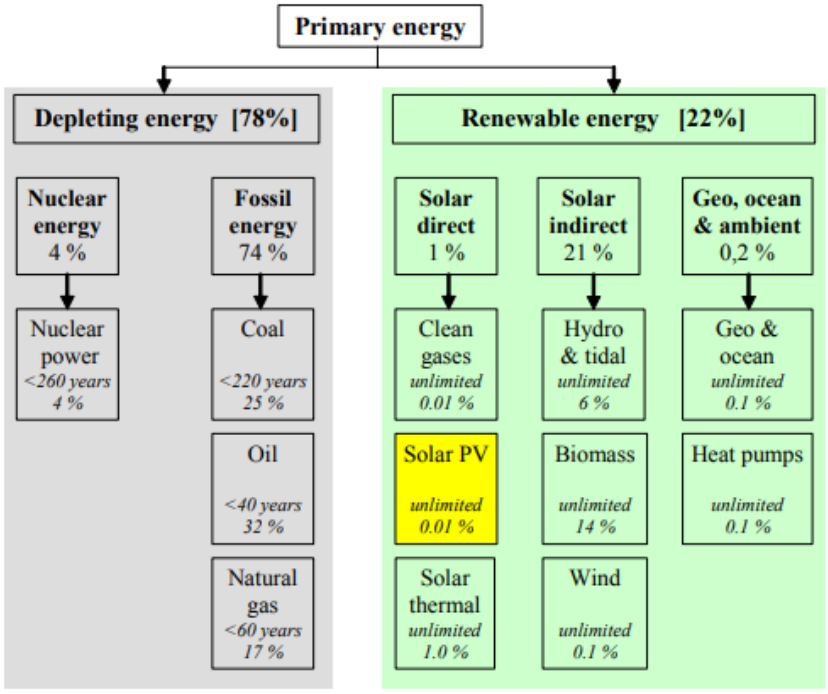

Figure 1.1: Today's energy distribution by sources [1]

In order to provide a rapidly growing population with high living standards, further economic development is essential. Further economic development requires more energy than we use today. The extra energy has to come from additional sources rather than only the traditional ones [1]. The necessity of developing an energy infrastructure, where so-called renewable or sustainable energy sources play the key role can be crucial in the nearest future if it is not already.

The usage of energy sources like nuclear energy and fossil fuels also inevitably results in vast amounts of greenhouse gas emissions as well as heat waste, which has an immense impact on the environment. The huge usage of these kinds of energy sources gradually changes the average temperature of the earth, the so-called global warming. Observations throughout the world make it clear that climate change is occurring, and rigorous scientific research demonstrates that the greenhouse gases emitted by human activities are the primary driver [2].

As is pictured in figure 1.2, the annual average temperature does increase over time.

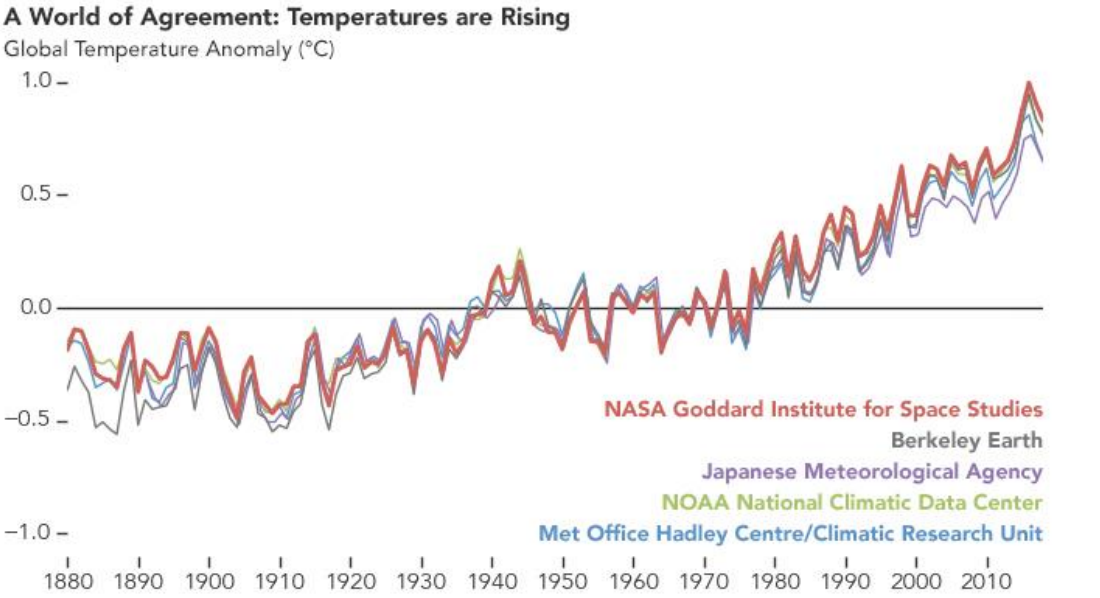

Figure 1.2: Global temperature anomaly (°C) [3]

The idea of using more and more (ideally – only) renewable energy sources, such as hydro, wind or solar energy is seen as one potential solution to overcome the dependence on non-renewable sources, thus mitigating the impact on the environment and making possible to supply with energy the increasing population.

There are plenty of challenges for the relatively young renewable energy field, starting from technological barriers up to the political issues with current monopolies of non-renewable sources-based energy providers. However, despite all the difficulties, those challenges can be overcome, and already now, some countries like Iceland, Sweden, and Costa Rica try to run on almost 100% renewables and eliminating fossil fuel usage within its borders.

1.2 Photovoltaics

One promising part of renewable energy sources is so-called photovoltaics, which generally describes systems that produce energy based on the photovoltaic effect. The phenomenon, when electric current and voltage are created in a material when it is exposed to light, is called photovoltaic effect. Photovoltaic systems are mostly describing a system consisting of solar panels, which are arrays of solar cells that generate current and voltage. The PV systems have plenty of advantages. Their eco-friendliness is very important because during their operation they do not produce any greenhouse gases, noise, or any other type of pollution and do not need fuel or water for operation. Also, they need very little maintenance and have a considerably long lifetime (10 to 20 years on average). Finally, because of its nature, the size of the production system can be very flexible, starting from a pocket-application up to a huge power plant with an area of 10 square kilometers [16]. Of course, they have their own disadvantages, such as high overall cost in comparison with regular energy sources, high dependence on weather conditions and geographic location, and lastly the necessity of having a large free area to fit solar panels.

Basis of a PV system is a solar cell, which is basically a simple semiconductor device that converts light into electric energy. Solar cells are usually divided into three main categories called generations up to recent years [4]. 1st -generation solar cells include single crystal solar cells and multi-crystal solar cells (generally, cells that use bulk crystalline silicon). This is the oldest type for solar cells and because of the high efficiencies is the most common type used. The 2nd generation solar cells are based on thin-film technology, and usually, CIGS, CdTe/CdS, and amorphous silicon are being used. They have lower costs and inferior efficiencies compared to 1st generation and can be grown on flexible substrates and on very large areas. The 3rd generation solar cells are focusing on achieving high efficiencies and can be made by different technologies, such as nanocrystal based solar cells, polymer-based solar cells, dye-sensitized solar cells, and concentrated solar cells.

1.3 Monograin layer solar cells

The solar cells used in this work are called monograin layer (MGL) solar cells. The MGL consists of a thick layer of powder crystals embedded into an organic resin. The MGLs combine the high photoelectronic parameters of single crystals and the advantages of polycrystalline materials such as low cost and simple technology of materials and devices, the possibility of making flexible devices, and the possibility of using of materials up to 100% [5]. However, it is important to note, that there are significant differences between MGL solar cells and idealized

devices, due to a high density of defect states in the absorber layer and parasitic losses connected with the device structure and contacts [6].

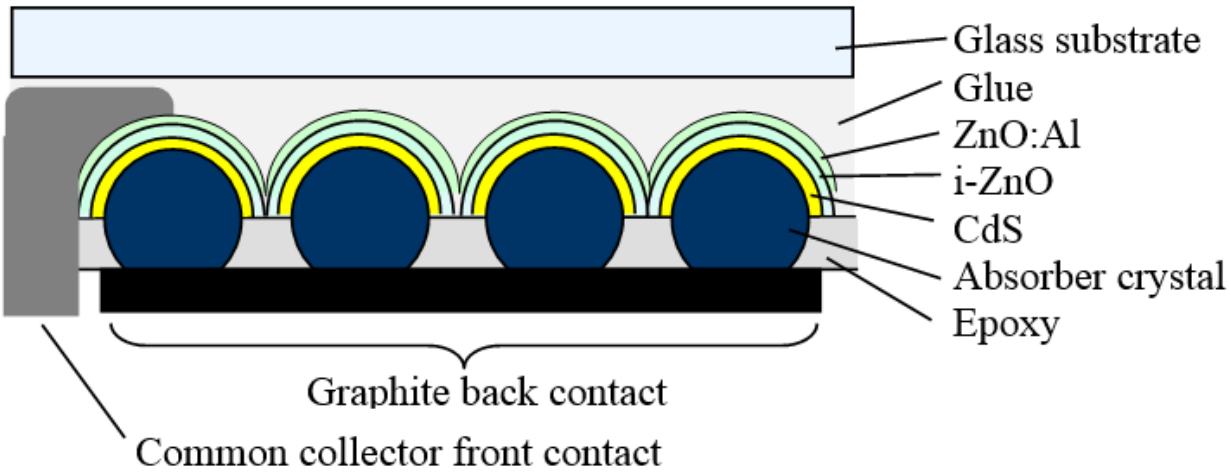

Figure 1.3: Schematic illustration of the studied CCGSe MGL solar cell structure [15]

There are various materials that can be used for the absorber layer, and one of those, that uses mostly low-cost, non-toxic, and earth-abundant elements is $Cu_2ZnSn(S,Se)_4$, also known as CZTS or CZTSe. This material has its own inherent challenges and difficulties, such as the formation of antisite defects – when Cu atoms occupy Zn sites and vice versa due to their similar atomic sizes, or stability issue – when CZTS breaks down at high temperatures due to Sn compounds being volatile. Despite the complexity, it's promising characteristics and optimal band gap value motivates research in the direction of improvements. In order to solve some of these issues, some elements in the compound can be changed, and in this work, zinc was replaced by cadmium, and tin was replaced by germanium. The difference in the ionic radii of copper and cadmium should prevent the formation of antisite defects and replacing tin with more stable germanium should solve the stability issue. The compound used for the absorber layer in the solar cells studied in this work is $Cu_2CdGeSe_4$, known as CCGSe.

Since the material is much less studied than more conventional ones, the prepared samples usually have low fill factor and efficiencies. However, research is constantly done in order to improve the performance of these cells, by trying different compounds or different treatments. In this work, 2 different samples (sample A and sample B) with different treatment methods are compared, to understand how another approach improves the performance. The main difference was the sulfurization of the surface of the absorber layer for one of the samples, which could lead to better device performance. Detailed description

of the sample preparation will be presented in chapter 3 of this work. The schematic of the sulfurization process can be seen on the figure 1.4.

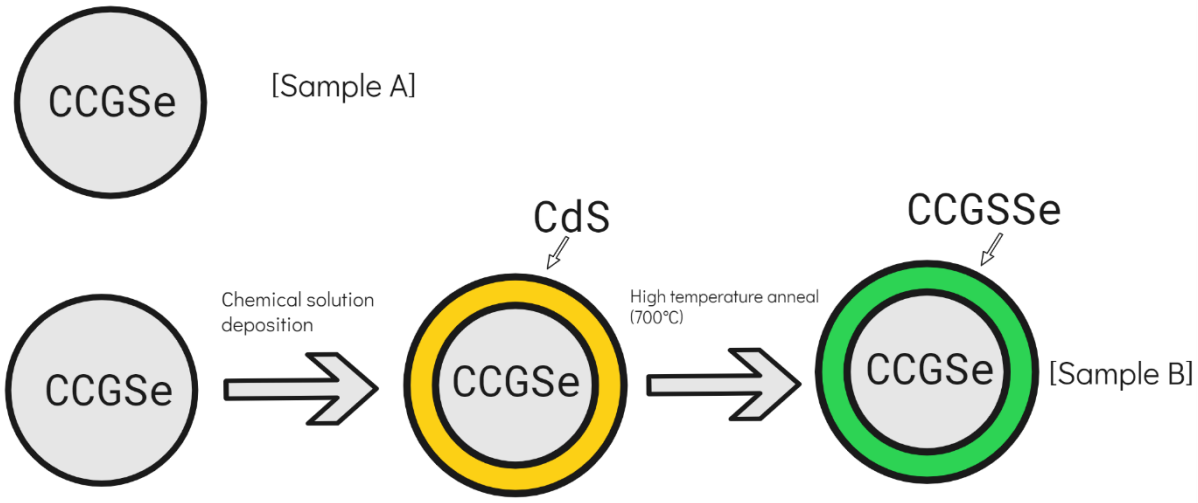

Figure 1.4: Schematic illustration of the sulfurization process

1.4 Aim of the study

In this work, temperature-dependent current-voltage (J-V) characteristics and external quantum efficiency (EQE) of 2 different samples of CCGSe-based MGL solar cells were studied. The work is aimed to find the diode circuit parameters (ideality factor and dark saturation current) and parasitic loss parameters (series resistance and parallel resistance) from J-V curves and study their dependences on temperature and light intensity. Based on the results, we can conclude if a new treatment method improved the performance of the solar cell.

The thesis consists of 4 main chapters. In the first 2 chapters the topic and appropriate theoretical background are introduced, in chapter 3 the experimental procedure is described, and finally, in chapter 4 the results are represented and discussed, followed by the conclusions.

Chapter 2 – Theoretical Background

2.1 Semiconductors

Semiconductors are generally materials that have electrical conductivity values falling between that of a metal and an insulator and consist of atoms that are from either group IV of the periodic table, from a combination of group III and group V (called III-V semiconductors), or of combinations from group II and group VI (called II-VI semiconductors). Unlike metals, the resistance of semiconductor material decreases with an increase of temperature, and their properties can be altered by doping when there are impurities added to the material.

In semiconductors, the band gap E_g, which is the energy difference between the conduction band and valence band, is relatively narrow (<2eV) [7], and the valence band is full, while the conduction band is empty. If the electron can emit a photon directly, the band gap is called direct, and if the electron needs to pass through an intermediate state before emitting a photon, the band gap is called indirect. Semiconductors can be classified as intrinsic or extrinsic. For an intrinsic semiconductor, there are only a few delocalized conduction electrons, the number of which increases exponentially with the increase in temperature. When it comes to an extrinsic semiconductor, the n and p are determined by the process called "doping" – when impurities are added to the material. Impurity atoms of elements with higher valency than the "host" element create an excess of electrons (n-type) and the ones with lower valency create bonds with missing electrons – "holes" (p-type).

2.2 Movement of electrical charge carriers

Electrical charge carriers (or just carriers) move freely throughout the semiconductor in random directions. Since the probability of any direction is equal, there is no net overall movement of carriers in any direction. As electrons are being considered as free carriers, their movement can be viewed as a movement in random direction with constant velocity, and because either direction has equally likely, the net displacement of the electron is zero.

When the semiconductor is exposed to light, the generation of carriers on the surface results in uneven distribution of carrier concentration throughout the material. This carrier concentration gradient will lead to diffusion of carriers from high concentration areas to low concentration ones, until with the time the distribution is even again. At higher temperatures, the diffusion has a higher rate, since the increase in temperature results in increased thermal velocities of carriers.

When the semiconductor is being affected by an electric field, a movement of carriers in a net direction occurs, which is called drift. The electrons have drift movement direction opposite to the electric field, while the holes drift in the direction of the electric field. As a result, the net current in the semiconductor is the sum of drift and diffusion currents.

2.3 Recombination

The process, when an electron is being stabilized back to the valence band is called recombination. The recombination process produces phonons (which most likely contribute to heat) and photons and is related to the lifetime of the product, which is a very important property for a solar cell application. There are 3 main types of recombination [8] - radiative recombination, Auger recombination, and Shockley-Read-Hall recombination.

In the case of radiative recombination, an electron from the conduction band directly recombines with a hole from the valence band – emitting a photon that has energy close to band gap energy value. Because of its nature, this recombination mechanism predominates in the direct band gap semiconductors[8].

Auger recombination is a non-radiative process involving three carriers. Direct Auger recombination occurs when an electron and hole recombine, but instead of producing light, either an electron is raised higher into the conduction band or a hole is pushed deeper into the valence band [18].

Shockley-Read-Hall (SRH) recombination occurs in not pure materials through defects and represents a two-step process. Firstly, an electron or hole is being trapped by an energy state in the forbidden region (those energy states can be created intentionally through doping or unintentionally). The occurrence of SRH recombination depends on the lifetime of electrons and holes in trap states. If the lifetime of one of the charge carriers is much shorter than that of the others, the probability of SRH will be low.

2.4 P-N Junction and solar cells

When p and n-type semiconductors are brought together, the p-n junction is formed, which is the basis for solar cells and other semiconductor electronics. During the formation of the p-n junction, when charge carriers move to other parts of the material, they leave exposed ionic cores, which create an electric field. This electric field keeps up the so-called depletion region, where there are few charge carriers, when the holes are in the p-type material, and the electrons are in the n-type material. So, when there is no voltage applied and assuming that the depletion region has been already established, there is no current flow across the junction.

Due to the diffusion of electrons and holes near the interface between n and p regions, a so-called "built-in" electric field appears. Depending on the direction of the battery induced electric field, the configuration can be "forward-biased" or "reverse-biased". If a positive voltage is applied to the p-type side and a negative voltage to the n-type side (figure 2.1.a), it will be forward-biased configuration, and the current will be able to flow (depending upon the magnitude of the applied voltage). If a negative voltage is applied to the p-type side and a positive voltage to the n-type side (figure 2.1.b), no (or exceptionally small) current flows. This configuration is called "reverse-biased" [9].

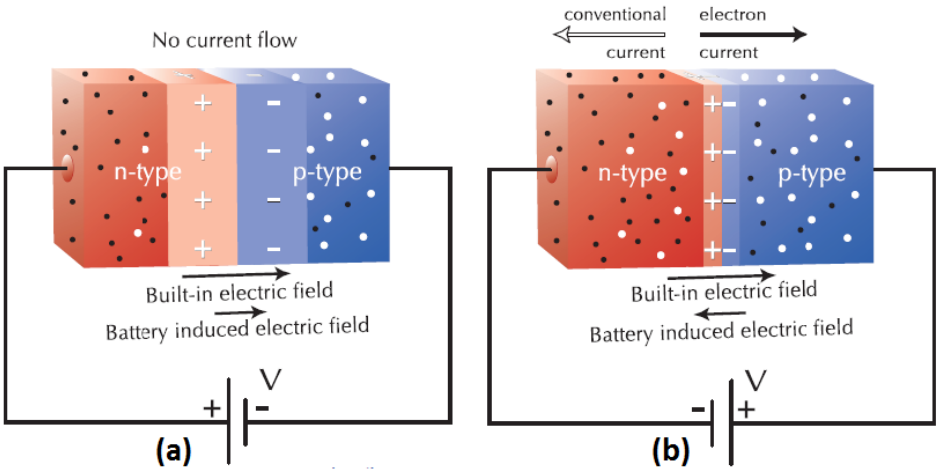

Figure 2.1: Forward (a) and Reverse (b) bias for a p-n junction [9]

If we are considering a solar cell, when there is no light applied, it behaves like a p-n junction diode. This kind of device is usually characterized by the current (or current density) and voltage dependence, the I-V, or J-V curves (figure 2.2).

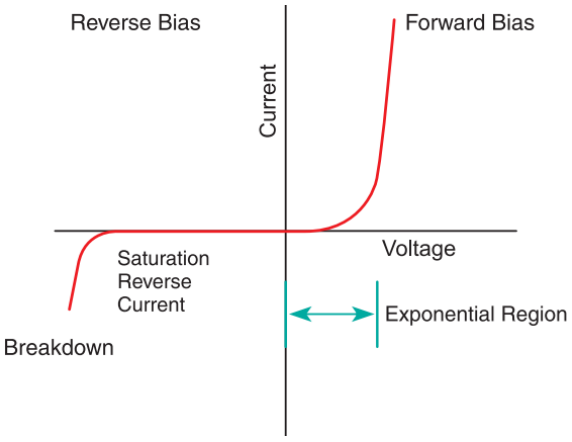

Figure 2.2: An I-V curve for silicon p-n junction diode [9]

In reverse bias, the positive voltage will attract electrons and repel holes, and the negative voltage will attract holes while repelling electrons, resulting in a minority carrier current, the reverse saturation current, which is normally very low and is almost constant. In case of too

high reverse bias voltage, the junction will breakdown and current flow will occur. In forward bias, the current increases exponentially with the increase in voltage.

2.5 Diode Equation and external circuit parameters

Mathematically, the net-current density is expressed as a function of voltage through the Shockley Diode Equation, which is a fundamental equation for microelectronics device physics. That describes the current-voltage behaviour of an ideal *p-n* diode [1].

$$J = J_o \left[\exp\left(\frac{qV}{KT}\right) - 1\right] \quad (2.1)$$

J is the net current density, q is the electron charge absolute value, V is the voltage applied across the diode, K is the Boltzmann constant, and T is the absolute temperature and J_o is the reverse saturation current density. When considering a solar cell, a term "dark saturation current" is used, since a solar cell behaves like a diode in the absence of illumination. It is also called the "recombination parameter" since it can be identified as the recombination current density in thermal equilibrium [10].

If considering a non-ideal, "real" diode, an ideality factor n is added to the equation (2.1).

$$J = J_o \left[\exp\left(\frac{qV}{nKT}\right) - 1\right] \quad (2.2)$$

The ideality factor represents to what extent the behaviour of the actual diode is comparable with the ideal diode behaviour, and has values varying between 1 and 2.

The dark saturation current can be represented as a function of temperature-dependent properties of a material[15]

$$J_o = A * T^2 \exp\left(-\frac{E_A}{nkT}\right) , \quad (2.3)$$

where A is a pre-exponential parameter, that includes Richardson constant.

When describing a solar cell under illumination, a photo-generation current will be added to the equation (2.2) [1].

$$J = J_o \left[\exp\left(\frac{qV}{nKT}\right) - 1\right] - J_{ph} \quad (2.4)$$

For an ideal solar cell, the n ideality factor will have a value of 1.

$$J = J_o \left[\exp\left(\frac{qV}{KT}\right) - 1\right] - J_{ph} \qquad (2.5)$$

As can be seen in figure 2.3, in the absence of light, the J-V curve of a solar cell is similar to a J-V curve of a diode. But when illuminated, the J-V curve goes down to the 4th quadrant, since the J_{ph} is added.

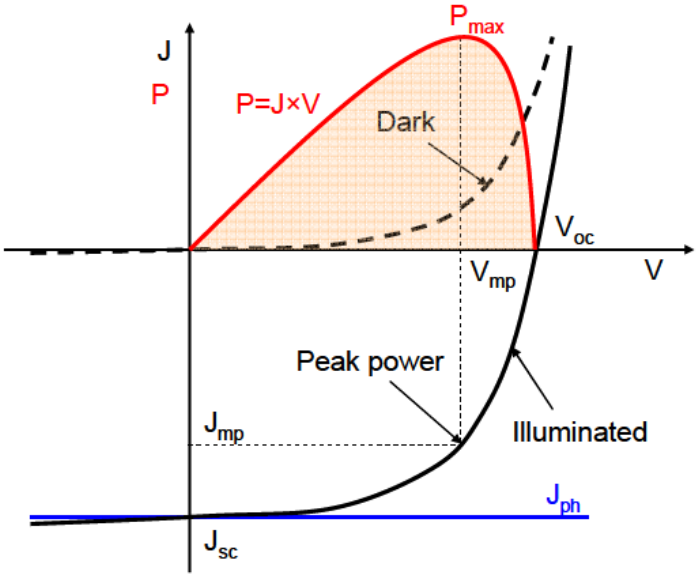

Figure 2.3: J-V characteristics of a solar cell in the dark and under illumination [1]

J-V curves are being described by using "external circuit parameters", such as open-circuit voltage V_{oc}, short-circuit current I_{sc} (with the respective J_{sc} short-circuit current density), maximal power P_{max}, fill factor FF and efficiency η.

V_{oc} is the maximal possible voltage delivery from a solar cell when the net current flow is zero. It can be calculated from formula (2.4) by taking J as 0 and rearranging the expression.

$$V_{oc} = \frac{KT}{q}\left(\frac{J_{ph}}{J_o} + 1\right) \qquad (2.6)$$

It can be seen from expression (2.6) that open-circuit voltage depends primarily on the photocurrent density and the recombination parameter.

I_{sc} is the short-circuit current, that is when the solar cell is short-circuited. The respective **J_{sc}** short-circuit current density is theoretically the maximum possible output from a solar cell, and in the idealized model is equal to the J_{ph}. It can be calculated from (2.5) by taking V as 0.

The power output P can be calculated by simple multiplication:

$$P = J \times V \qquad (2.7)$$

The point, where the power output has maximal value, is called maximal power $\mathbf{P_{max}}$, with the corresponding $\mathbf{J_{mp}}$ maximum power point current density and $\mathbf{V_{mp}}$ maximum power point voltage.

The ratio between the maximal power and the multiplication of short-circuit current density and open-circuit voltage is called Fill Factor.

$$FF = \frac{P_{max}}{J_{sc}\,V_{oc}} = \frac{J_{mp}\,V_{mp}}{J_{sc}\,V_{oc}} \tag{2.8}$$

Finally, efficiency is defined as the following ratio

$$\eta = \frac{P_{max}}{A_c\,E} = \frac{J_{sc}\,V_{oc}\,FF}{A_c\,E}, \tag{2.9}$$

where A_c is the area of the cell and E is the incident radiation flux, which in the standard test conditions is usually taken with the value of 1000 W/m^2.

From (2.8) and (2.9) it is easy to express the FF through efficiency.

$$FF = \frac{A_c\,E}{J_{sc}\,V_{oc}} \times \eta \tag{2.10}$$

When it comes to the ideality factor and dark saturation current estimation, there are different methods, and one of those is the so-called "J_{sc}-V_{oc} method"[15]. For this method, we have to measure the J_{sc} and V_{oc} at different illumination intensities and compare these measurements done at different temperatures. If we take the equation 2.4 and give J and V values of 0 while approximating $J_{sc} = J_{ph}$, we will obtain

$$J_{ph} = J_o\left[\exp\left(\frac{qV_{oc}}{nKT}\right) - 1\right] + \frac{V_{oc}}{R_p} \tag{2.11}$$

In this formula, R_p shunt resistance is used, which will be described in the next part of the chapter. Using formula 2.11, it is possible to estimate the n and J_o. If we make a plot of ln(Jsc) versus Voc, it should be a straight line, and from the slope, the n is being calculated, and Jo is being estimated from the intercept of the line with the J_{sc} axis. An example is the 4.7 figure, where this method was applied.

2.6 Loss mechanisms and modelling of the equivalent circuit

Solar cell operation can be characterized by identifying loss mechanisms. The loss mechanisms can be divided into three main categories. First, recombination losses limit the V_{oc}. Second, parasitic losses, such as series resistance, shunt resistance, and voltage-dependent current collection that primarily impact the FF, but can also reduce J_{sc} and V_{oc}. Finally, optical losses limit the generation of carriers and, therefore J_{sc} [15]. Optical losses include losses due to non-

absorption of long wavelengths, thermalization of the excess energy of photons, and incomplete absorption due to the finite thickness of the absorber layer [1].

The non-absorption and thermalization are both related to the spectral mismatch, that is, when photons have too high or too low energy values, compared to the absorber material's band gap energy value. A photon with the excess of energy will create an excess of heat in the crystal lattice in the process of thermalization, while the photons with energy smaller than E_g of the absorber won't have a contribution in the conversion process.

The finite thickness of the absorber material is another reason for losses, the incomplete absorption, which is characterized by the QE_{int} internal quantum efficiency. Generally, the quantum efficiency QE is a dimensionless parameter, given by the number of electrons that exit the device per incident photon at each wavelength [11]. QE_{int} doesn't include the optical losses, while the external quantum efficiency EQE includes them also.

The behaviour of a solar cell can be described by modelling an equivalent circuit as pictured in figure 2.4.

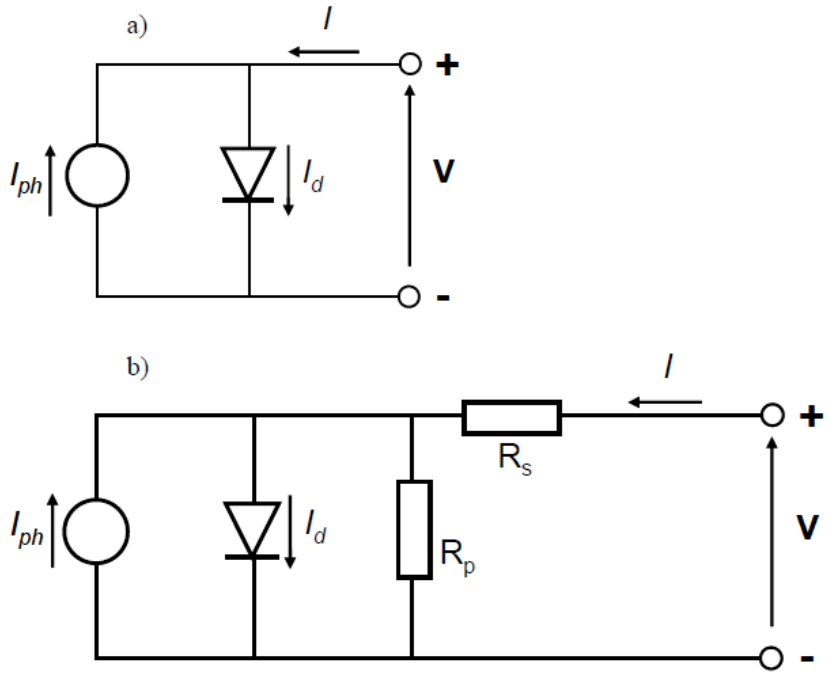

Figure 2.4: a) The equivalent circuit of an ideal solar cell. b) The equivalent circuit of a solar cell with series resistance R_s and shunt resistance R_p [1]

The diode is being formed by the p-n junction, and that diode and the current source are in parallel connection. The *J-V* characteristic of the one-diode equivalent circuit with the series resistance and the shunt resistance is described by formula (2.12) [1].

$$J = J_o \left[\exp\left(\frac{q(V-R_sJ)}{nKT}\right) - 1\right] + \frac{(V-R_sJ)}{R_p} - J_{ph} \qquad (2.12)$$

Series resistance in a solar cell has three causes: firstly, the movement of current through the emitter and base of the solar cell; secondly, the contact resistance between the metal contact and the absorber material; and finally, the resistance of the top and rear metal contacts. The main impact of series resistance is to reduce the fill factor, although excessively high values may also reduce the short-circuit current. Also, significant power losses can occur due to low shunt resistance, which provided an alternate current path for the light-generated current. The effect of shunt resistance is particularly severe at low light levels since there will be less light-generated current. The loss of this current to the shunt, therefore, has a larger impact. In addition, at lower voltages where the effective resistance of the solar cell is high, the impact of resistance in parallel is large [12].

Ideally, the R_s is considered 0, and practically the larger its value - the larger the deviation from a J-V curve of an ideal solar cell. As can be seen in figure 2.5.a, the open-circuit voltage is not being affected by the series resistance. When it comes to the shunt resistance, the situation is the opposite. As figure 2.5.b depicts, the J-V curves deviate further away from an ideal curve with the decrease of R_p value. R_s and R_p are often generally described with the term "parasitic resistances". For R_s, a typical value is in range of 0.5-1.3 kΩ*cm^2, while for R_{sh} it is around 1 kΩ*cm^2[12].

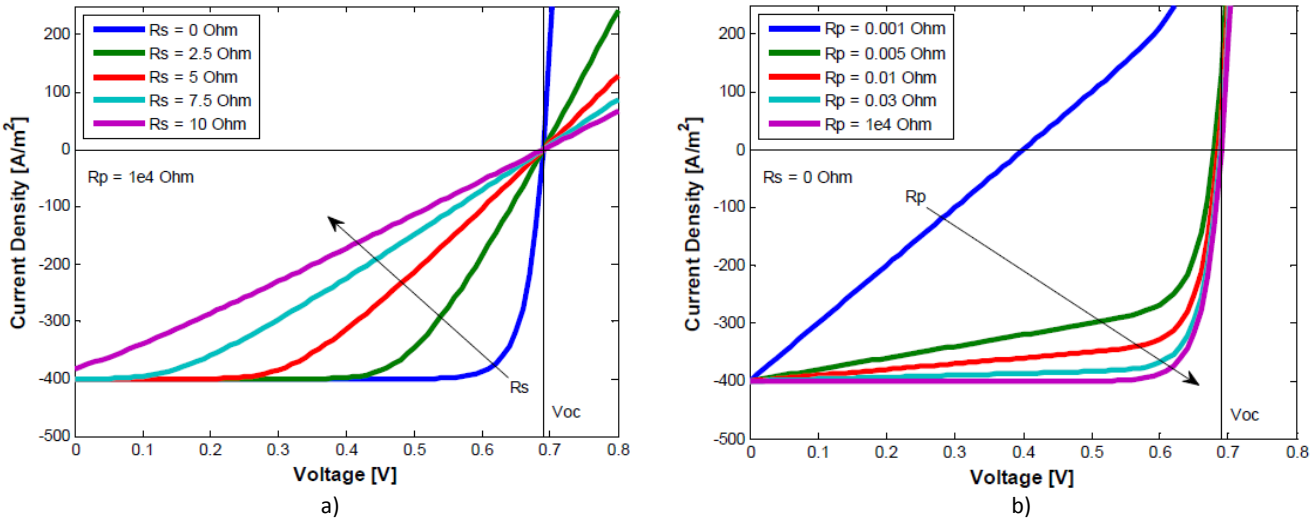

Figure 2.5: Effect of series(a) and shunt(b) resistances on the J-V characteristic of a solar cell [1]

In practical solar cells, the *FF* is influenced by the additional recombination occurring in the p-n junction. This non-ideal diode is often represented in the equivalent circuit by two diodes, an ideal one with an ideality factor equal to one and a non-ideal diode with an ideality factor greater than one. The equivalent circuit of a practical solar cell is presented in figure 2.6.

The *J-V* characteristic of the two-diode equivalent circuit is described by formula (2.11) [1]:

$$J = J_{d1}\left[\exp\left(\frac{q(V-A_cJR_s)}{n_1KT}\right)-1\right]+J_{d2}\left[\exp\left(\frac{q(V-A_cJR_s)}{n_2KT}\right)-1\right]+\frac{V-A_cJR_s}{R_p}-J_{ph} \qquad (2.13)$$

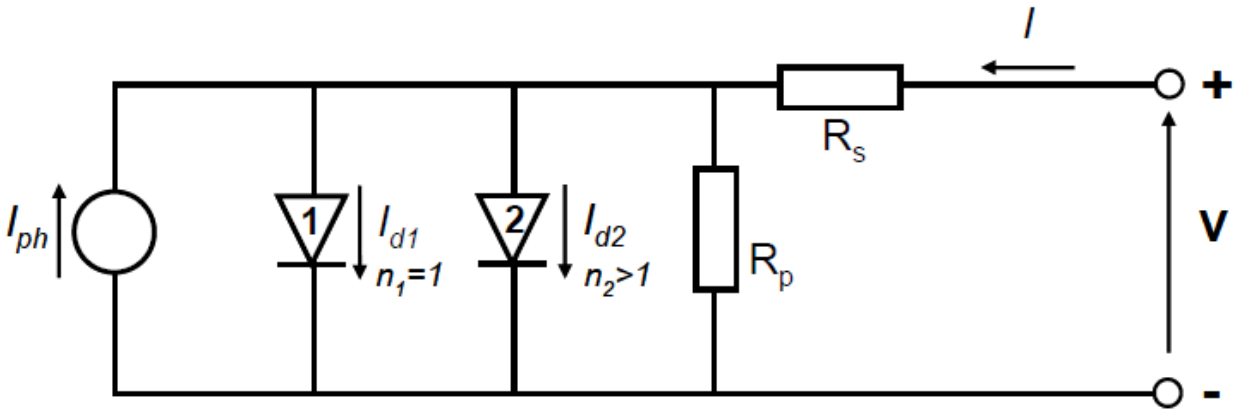

Figure 2.6: The equivalent circuit of a solar cell based on a two-diode model [1]

J_{d1} and J_{d2} are the dark saturation currents for 1st and 2nd diodes, and their ideality factors are n1 and n2 respectively.

The ideality factor can be defined as a measure of the junction quality and the type of recombination in a solar cell. For the thermionic emission, the n has a value of 1. However, some recombination mechanisms, particularly if they are large, may introduce an ideality factor of 2. A high value of n not only degrades the FF but since it usually indicates high recombination, it gives low V_{oc} as well [15]. It can be calculated by different means, and one of those is the so-called "shading method" described in the paper of S. Bowden and A. Rohatgi[19], which proposes a method of estimation for external circuit parameters by measuring I-V curves in different illumination conditions.

$$n = \frac{V_{oc(full)}-V_{oc(shaded)}}{\ln(I_{sc(full)})-\ln(J_{sc(shaded)})} * \frac{q}{KT} \qquad (2.14)$$

2.7 The influence of external parameters of a solar cell on J-V curves

Apart from the internal parameters, that are determined by the solar cell itself, the J-V curves are being influenced also by external parameters, such as temperature and radiation level. Like all other semiconductor devices, solar cells are sensitive to temperature. An increase in temperature reduces the band gap of a semiconductor, thereby affecting most of the semiconductor material parameters. The main temperature dependence in solar cells arises from the variation of three main parameters: J_{SC}, V_{OC}, and FF. The parameter most affected by the change in the temperature is V_{OC} [15].

Generally, the short-circuit current density increases slightly with the temperature increase, since the band gap energy decreases, and more photons have enough energy to create e-h pairs [12]. As was stated previously, V_{oc} open-circuit voltage depends primarily on the J_{ph} photocurrent density and J_o recombination parameter. The recombination parameter in its turn can be represented as a function of the band gap of the material – decreasing the band gap energy value increases J_o. This can explain the significant drop in V_{oc} shown in figure 2.7 since by increasing the temperature we decrease the band gap energy, which results in increased J_o, which lowers the V_{oc}.

We can obtain V_{oc} if we take the equation 2.12, give the J value of 0, and rearrange the equation.

$$V_{oc} = \frac{nKT}{q}\, ln\left(1 - \frac{V_{oc}}{R_{sh}J_0} + \frac{J_{ph}}{J_o}\right) \tag{2.15}$$

The temperature dependence of the V_{oc} and J_{sc} for the studied samples under constant illumination can be seen on the figures 2.7 and 2.8.

It can be seen on the figures, that there is an increase in short-circuit current density and a decrease in open-circuit voltage when increasing the temperature.

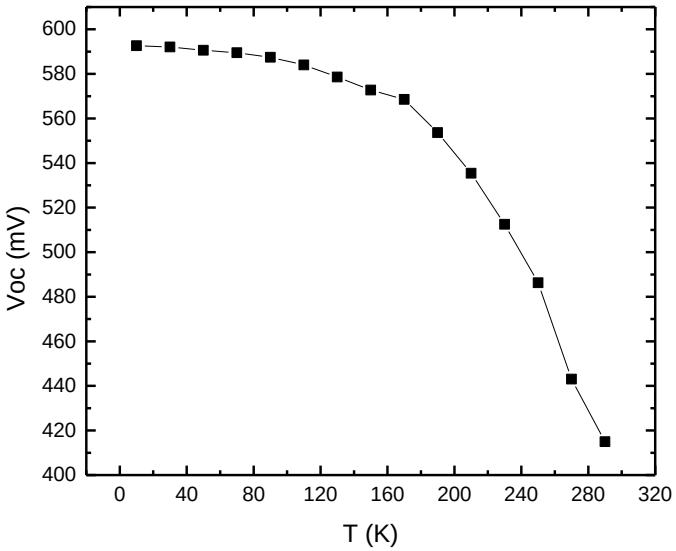

Figure 2.7: Temperature dependence of V_{oc} open-circuit voltage of one of the studied CCGSe MGL solar cells.

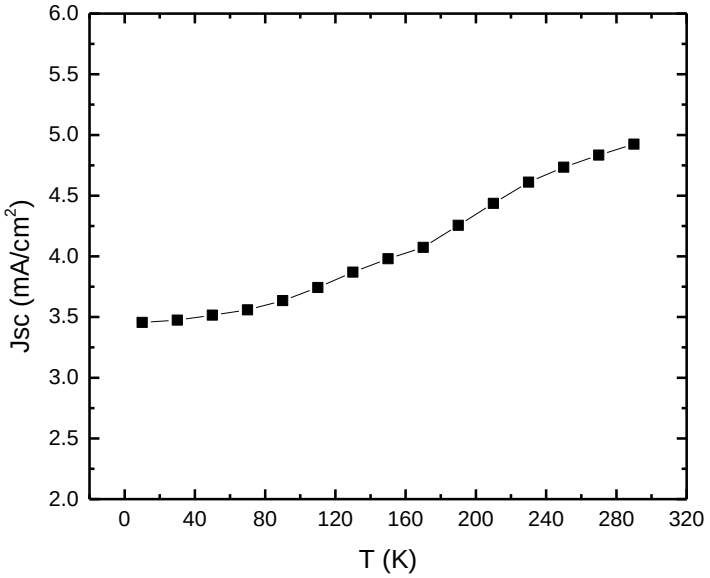

Figure 2.8: Temperature dependence of J_{sc} short-circuit current of one of the studied CCGSe MGL solar cells.

When it comes to the dependence on the light intensity, the picture is opposite (fig. 2.9) - a big drop in short-circuit current density occurs when decreasing the light intensity, while the drop in open-circuit voltage is relatively small.

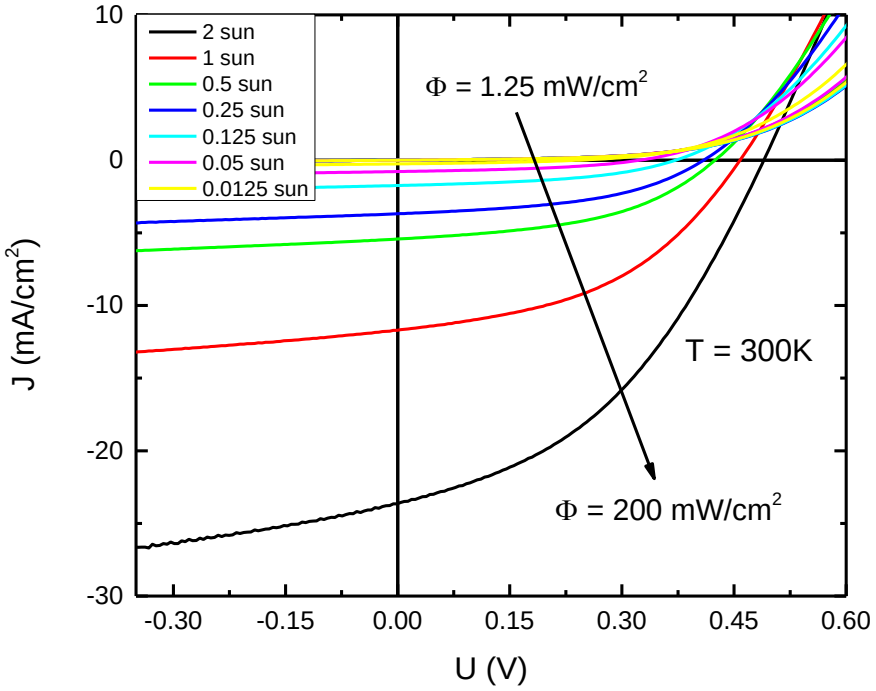

Figure 2.9: The light intensity dependence of the J-V curves of one of the studied CCGSe MGL solar cells at 300K temperature.

2.8 Quantum Efficiency analysis

The "quantum efficiency" (QE) is the ratio of the number of carriers collected by the solar cell to the number of photons of a given energy incident on the solar cell. The quantum efficiency may be given either as a function of wavelength or as energy. If all photons of a certain wavelength are absorbed and the resulting minority carriers are collected, then the quantum efficiency at that particular wavelength is unity[20].

Quantum efficiency measurements can be used to characterize solar cell's photocurrent collection and estimate the electronic and optical losses in the device. Normally when discussing quantum efficiency, two different types are discussed: *External Quantum Efficiency* (EQE) and *Internal Quantum Efficiency* (IQE). EQE includes the effect of optical losses such as transmission and reflection. IQE refers to the efficiency with which photons that are not reflected or transmitted out of the cell can generate collectable carriers[20].

In this work, EQE has been studied with varying the temperature. Studying the difference between the ideal square QE shape and the actual curve allows us to estimate the losses.

The quantum efficiency of a solar cell can be calculated from the equations for minority carrier continuity and current density[15]

$$QE \cong 1 - \frac{\exp(-\alpha W)}{\alpha L_{eff}+1} \tag{2.14}$$

where α is the absorption coefficient for wavelength λ, W is the depletion width, and L_{eff} is the effective diffusion length for electrons in the absorber after correction for the finite thickness of the absorber.

Chapter 3 – Experimental Procedure

The CCGSe powder materials used for solar cells studied in this work were synthesized from commercially available CdSe, self-synthesized CuSe, elemental Ge powder, and Se shots in the liquid phase of flux materials in evacuated quartz ampoules. Potassium iodide (KI) – was used as flux material with a ratio of 1:1 [17]. More information about synthesis can be found in the above-mentioned article [17].

For the preparation of the MGL solar cells, post-treated powder crystals were covered with chemical bath deposited CdS buffer layers. For MGL formation, a monolayer of kesterite type powder crystals was embedded into a thin layer of epoxy such that the upper part of each grain sticks out of the polymer film. After polymerization of this epoxy, i-ZnO and conductive ZnO:Al were deposited by radio frequency (RF) sputtering onto the open (i.e., not covered by epoxy) surface of the layer. Finally, the glass substrate was glued onto the front surface of the MGL membrane, and the back contact area of crystals was opened by chemical etching and by additional abrasive treatment methods. Graphite paste was used to apply the back contacts. The analysis area of the solar cell is determined by the back contact area, which is typically about 0.04 cm^2. The active area of the MGL solar cells is around 75% of the total analysis area. The other 25% of the total area, comprising epoxy between the absorber crystals, is passive [15].

In this work, the measurements are done for two types of solar cells – sample A and sample B. Both are similar types of solar cells, but with differences in the post-treatment step for sample B. Both materials were chemically etched and annealed in vacuum, sample A at 400 C for 2 hours, and sample B was first covered with CdS and then annealed at 700C for 1 hour. For sample B the last step is nano-scale sulfurization of the surface of the absorber layer, which may lead to enhanced device efficiency via band gap widening at the surface [23]. More details about the nano-scale sulfurization of the absorber layer process can be found in the article [23].

For J-V measurements, a galvanostat/potentiostat Autolab PGSTAT30 was used as a source meter, a standard halogen lamp was used as a light source and spectrally net filters were used to control the light intensity. The same Autolab PGSTAT30 was used also for EQE measurements, as a potentiostat/current amplifier. Apart from the same halogen lamp, a computer-controlled prism monochromator Carl Zeiss SPM-2 was used for EQE measurements. Temperature-dependent measurements for both J-V and EQE were done with a closed-cycle Helium cryostat Janis, that allows temperature range from 10K up to 325K.

Chapter 4 – Results and Discussion

4.1 Temperature and light intensity-dependent J-V analysis of CCGSe MGL solar cells

The results of temperature-dependent J-V measurements are in good accordance with theory, since there is a well visible decrease in V_{oc} and an increase in J_{sc} with the increase in temperature, as can be seen in graph 4.1.

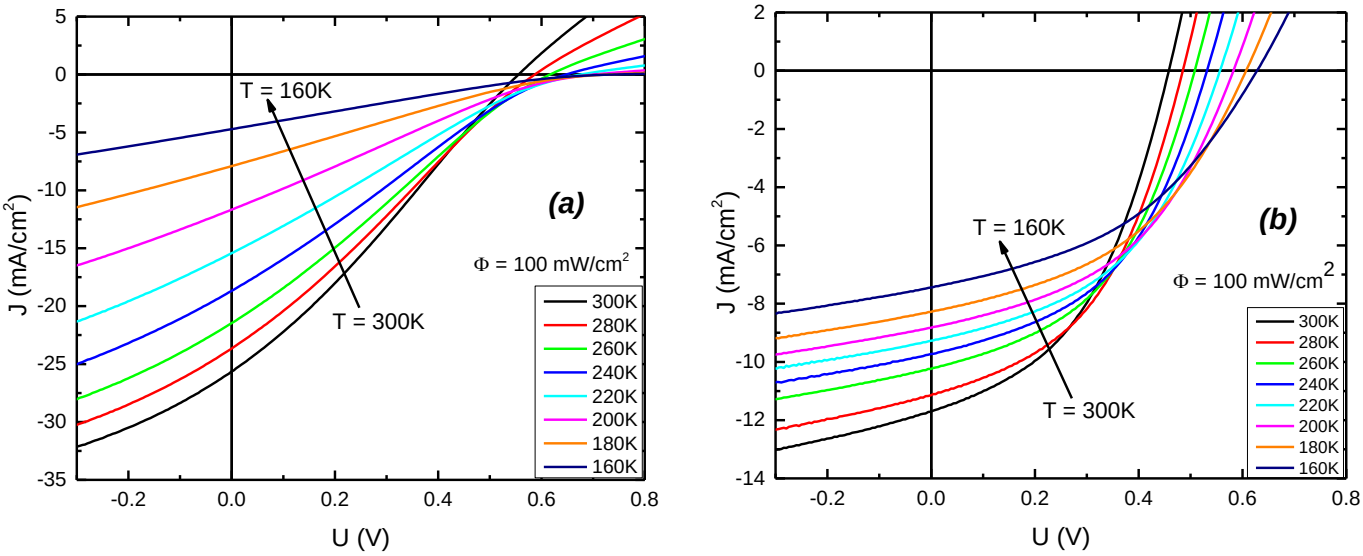

Figure 4.1: The temperature-dependent J-V curves of the studied CCGSe MGL solar cells at a fixed light intensity of 100 mW/cm². (a) – sample A, (b) – sample B.

From the comparison of these graphs, it can be seen that: the absolute current is different, with the sample A having a maximal current density of around 26 mA/cm², while sample B had a maximal current density of around 12 mA/cm²; the shape (the squareness) of the J-V curves is much different - sample A has very low FF – around 26%, and with decreasing temperature it gets lower, as low as 20% and also the J_{sc} drops drastically, while sample B has better FF of around 45% and J-V curves show diode behaviour. To have a better understanding and explain the reason behind this kind of different performance of the solar cells, it is important to extract the J-V curve parameters. This can be done with several methods, and in this work, it is done mainly by using 2 methods – fitting the theoretical solar cell equation (2.10) to the experimental data in the least-squares fitting method and the estimation process described in the article of S. Bowden and A. Rohatgi[19], which will be named in this work as “shading method”.

The results of the parameter extraction can be seen in the following graphs.

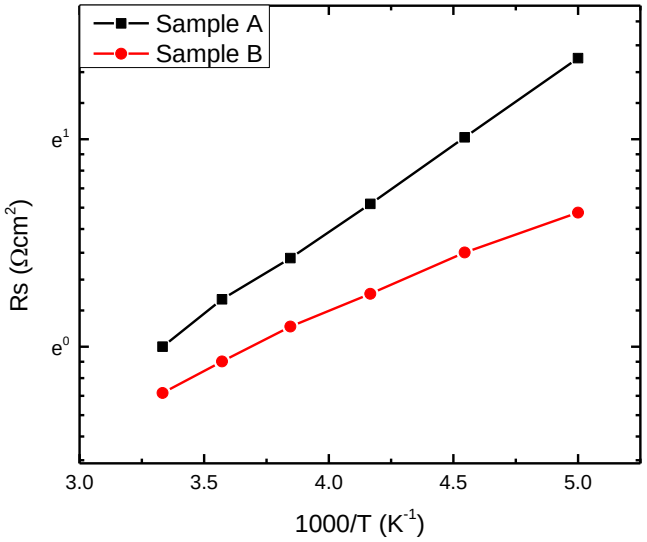

Figure 4.2: The temperature dependence of R_s series resistance of the studied samples in the temperature range of 300-200K.

Sample B has lower series resistance around 1 Ω/cm^2 at room temperature, while sample A has 0.8 Ω/cm^2, and this difference becomes even more significant at lower temperatures, which should allow sample B to have a higher current flow, theoretically speaking. However, the actual current of the latter is lower due to other factors. The results shown in figure 4.2 are coinciding with the theory, since increasing the temperature should decrease the resistivity of a semiconductor. The difference in the shape of the J-V curves, which was pointed out earlier, can be explained by the difference in shunt resistance, represented in figure 4.3.

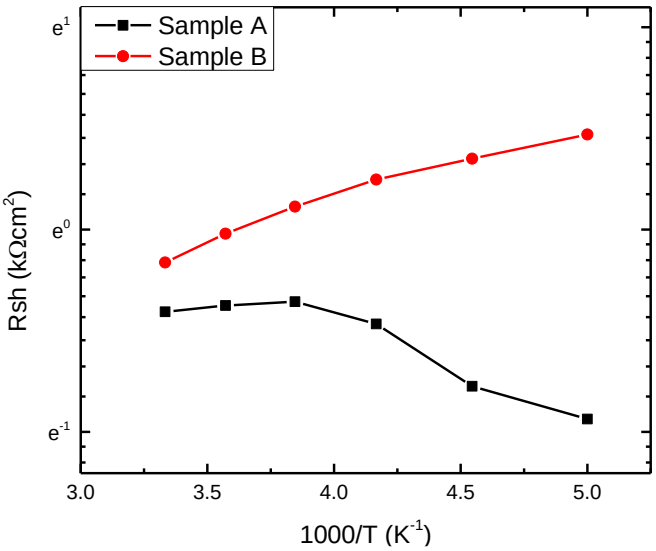

Figure 4.3: The temperature dependence of R_{sh} shunt resistance of the studied samples in the temperature range of 300-200K.

The shunt resistance of sample A is initially lower than that of sample B, around 0.66 kΩ*cm^2 compared to 0.85 kΩ*cm^2 and it drops even more when going to lower temperatures, which results in low FF and little to no sign of diode behaviour of J-V curves. The shunt resistance of sample B, on the other hand, has higher initial shunt resistance, and it raises when decreasing the temperature, preventing the cell form shunting and resulting in higher FF and J-V curves with characteristic diode behaviour. However, both of these values are still lower than the suggested R_{sh} value which is around 1 kΩ*cm^2[12]. Generally, the temperature dependence of a semiconductor's resistivity is described in the Arrhenius form: $\sigma(T) = \sigma_o \exp(-E_a/KT)$, where σ is the conductivity of the semiconductor, and σ_o is a preexponential factor.

The thermal dependence of the Fill Factor can be seen in the following graph.

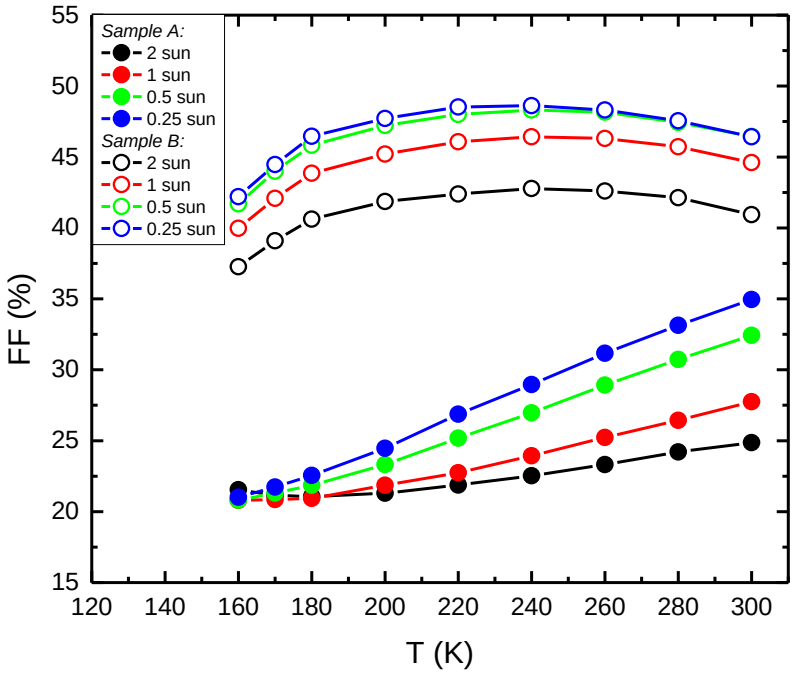

Figure 4.4: The temperature dependence of the fill factor of the studied samples.

As we can see in figure 4.4, in both cases, the trend for intensity dependence is similar: lowering the light intensity leads to an improvement in fill factor. However, there is a difference in the temperature dependence for the samples, with the sample A being strongly affected by temperature and its FF dropping significantly in low-temperature range, and sample B having comparatively stable FF, and even increasing in the range of 300K-240K.

In order to obtain the activation energies and compare them with the band gap energies, the thermal behaviour of the V_{oc} open-circuit voltages under different illumination conditions was studied, as is presented in the next figure 4.5.

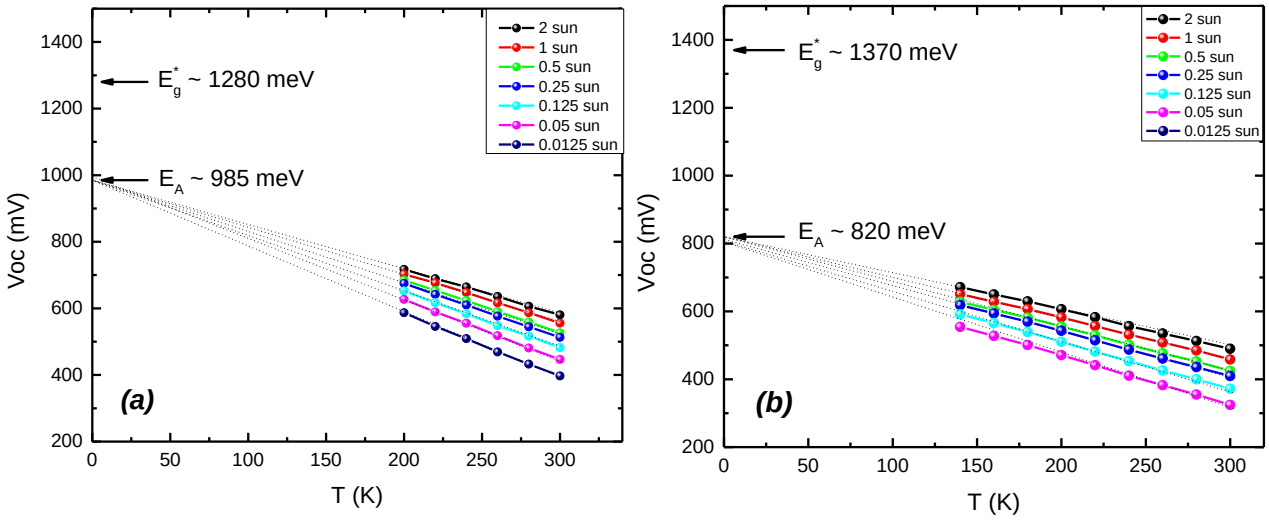

Figure 4.5: The temperature dependence of V_{oc} open-circuit voltages of the studied samples. (a) –sample A, (b) – sample B.

The effective band gap energy (E_g^*) values are used as reference points on the V_{oc} axes (Fig. 4.5) and were obtained from the temperature-dependent external quantum efficiency measurements, discussed later in this work. According to theory[15], from the extrapolation of $V_{oc}(T)$, the activation energy E_A can be determined at T = 0 K. However, this method can be considered reliable only when the ideality factor does not depend on the temperature. It can be seen on figure 4.6, that even though there is some temperature-dependent variation for the value of n, it can be considered constant in frames of an approximation, which will allow estimating the activation energies for both samples.

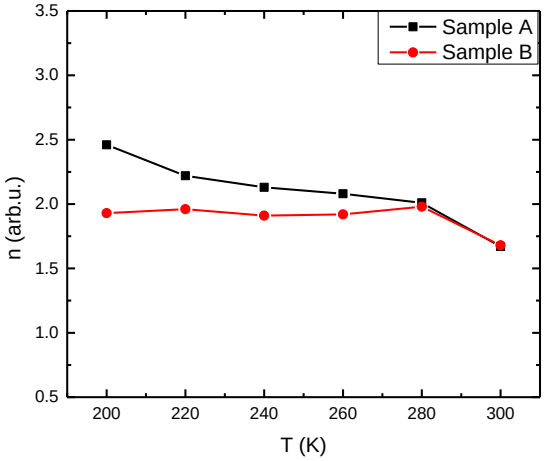

Figure 4.6: The temperature dependence of the ideality factor n of the studied samples.

These values for n were estimated using the so-called “shading method” mentioned before in the second chapter of this work. However, the ideality factor can be calculated alongside the dark saturation current (J_o) using the J_{sc}-V_{oc} method, and it will be noted as n’.

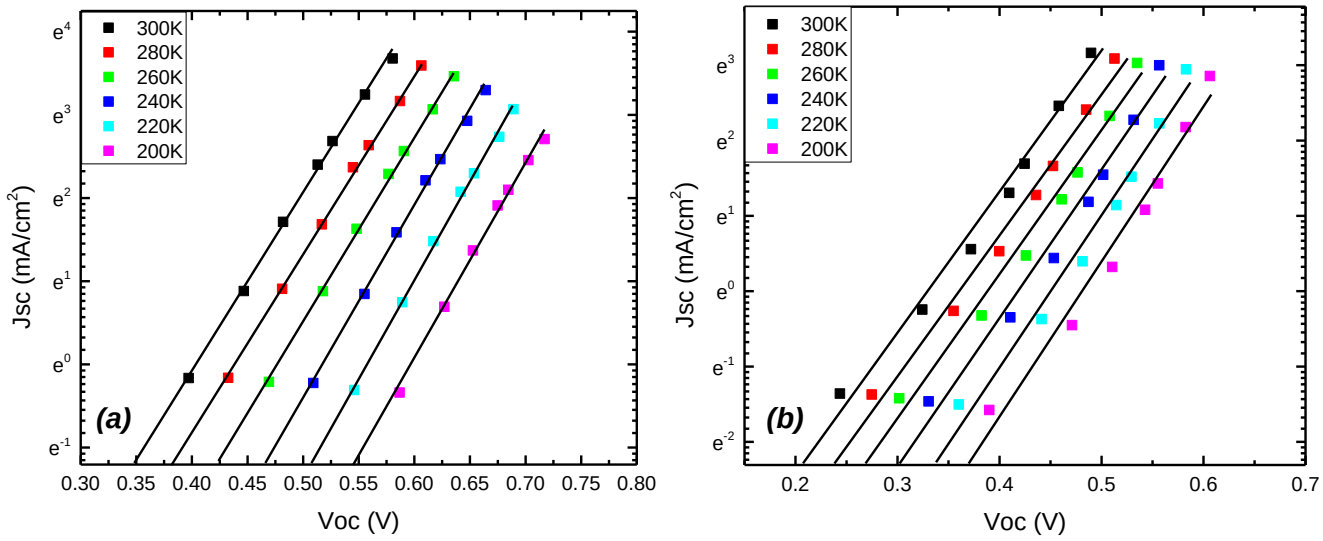

Figure 4.7: The J_{sc}-V_{oc} curves of the studied samples. The curves were constructed by plotting J_{sc} values versus V_{oc} in the temperature range of 300K-200K by varying the illumination intensity from 1.25mW/cm² to 200mW/cm². (a) – sample A, (b) – sample B.

As can be seen in figure 4.7, the data shows exponential behaviour, confirming the theoretical approach, described in the 1st chapter of this work. From the slope, the n’ was calculated, and from the intercept with the J_{sc} axis, J_o was estimated. The results are shown in figure 4.8.

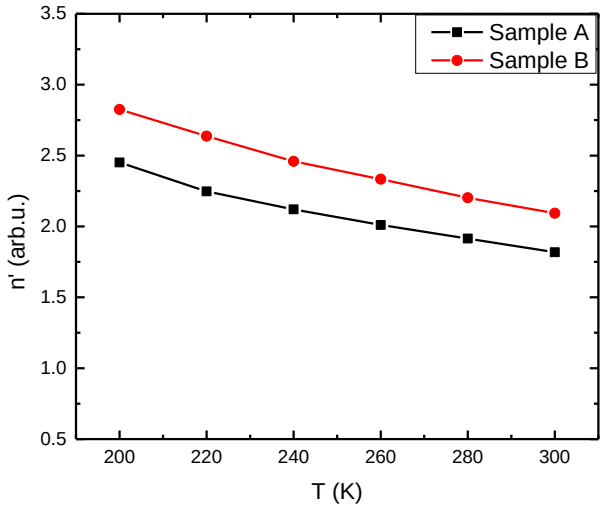

Figure 4.8: The temperature dependence of the ideality factor n’ of the studied samples obtained from the J_{sc}-V_{oc} method.

It is interesting to note, that the estimated values for n and n' are very close in case of sample A, while for sample B the values have a difference, with the n' estimated by *the* J_{sc}-V_{oc} method being higher. For the dark saturation current, the following results were obtained

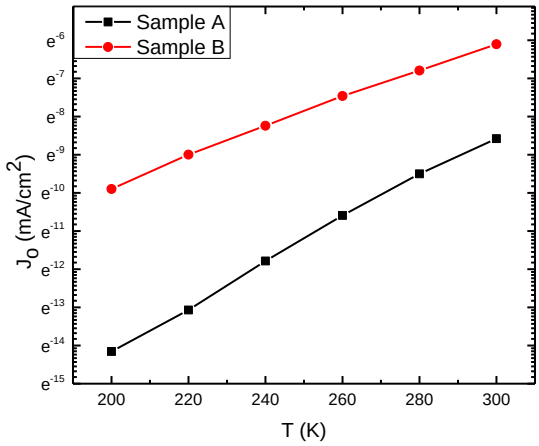

Figure 4.9: The temperature dependence of J_o dark saturation current of the studied samples obtained from the J_{sc}-V_{oc} method.

Apart from studying a solar cell's performance in illuminated conditions, it can be also studied how it behaves in the dark – analyzing the so-called dark J-V curves, as shown in figure 4.10.

By studying the J-V curves obtained without illumination, we can avoid a significant amount of noise and perturbation of data.

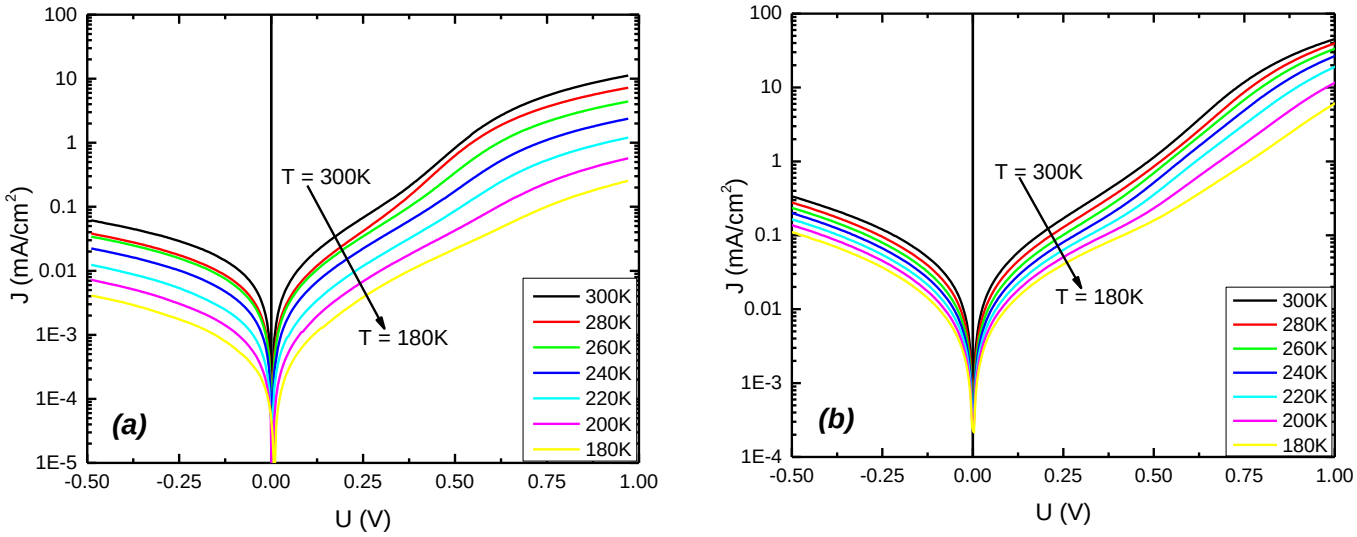

Figure 4.10: The temperature dependence of dark J-V curves of the studied samples. (a) – sample A, (b) – sample B.

By fitting the obtained data to the (2.10) solar cell equation (since the curves were obtained from measurements in the dark - J_{ph} must be taken as 0) we can estimate the external circuit parameters. The results can be seen in figure 4.11.

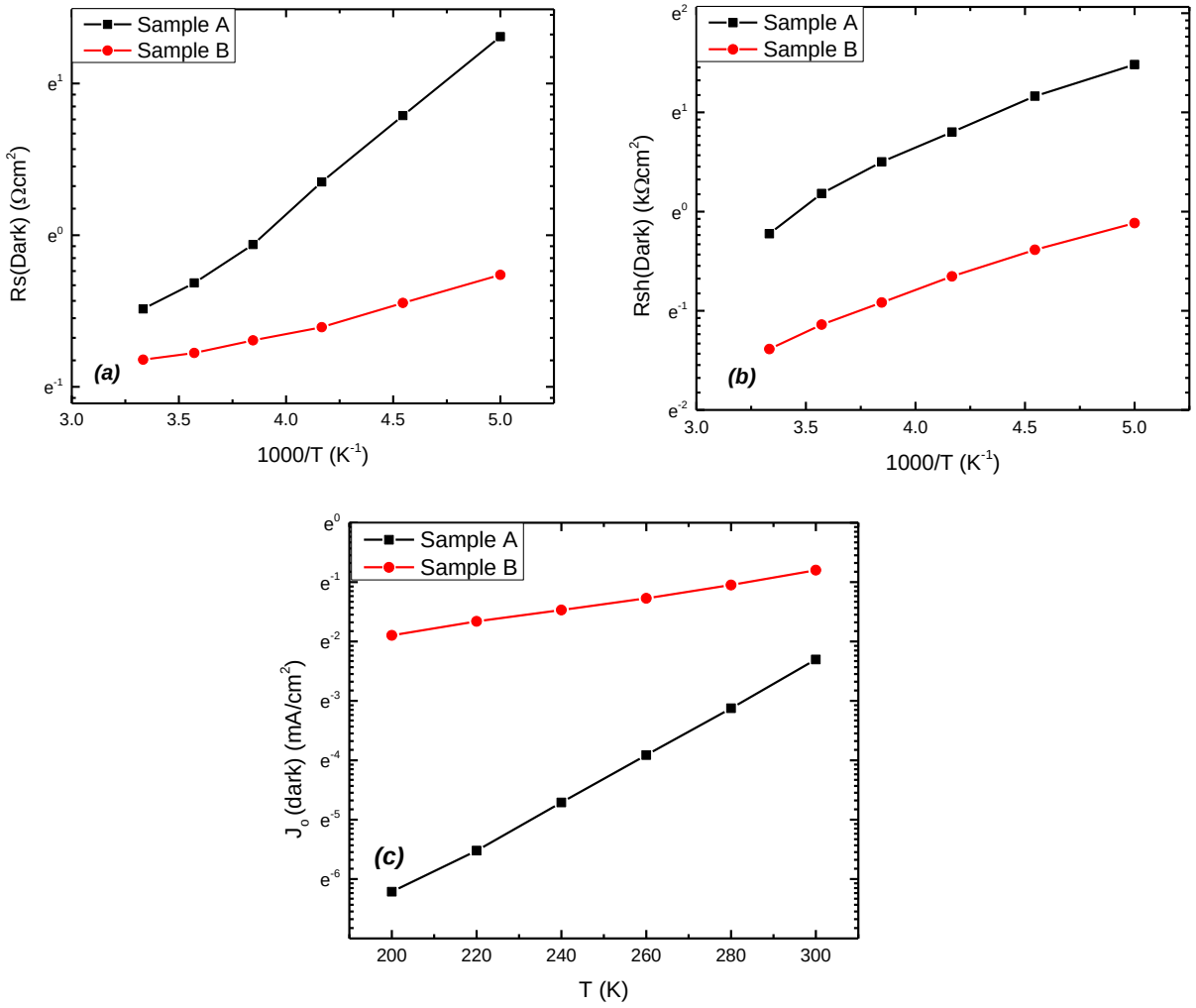

Figure 4.11: The temperature dependence of R_s series resistance(a), R_{sh} shunt resistance(b), and J_o dark saturation current(c) of the studied samples obtained from the dark J-V curves in the temperature range of 300-200K.

By fitting the obtained values of dark saturation current to the equation (2.3), it is possible to estimate the E_A activation energy value. For sample A, E_A was estimated to be 1eV from J_o values and 0.94 eV from J_o^{dark}, which is close to the 0.985 eV obtained from the J_{sc}-V_{oc} method. For sample B, E_A was estimated to be 0.85eV from J_o values and 0.79 eV from J_o^{dark}, which is also close to the value obtained from the J_{sc}-V_{oc} method - 0.82 eV. Additionally, it can be easily noticed that the dark saturation current is much higher for sample B, which indicates on high recombination current resulting in high V_{oc} losses. Limited V_{oc} in its turn results in significantly less current output in comparison with sample A.

4.2 Temperature-dependent EQE analysis of CCGSe MGL solar cells

In the following paragraph, the results of temperature-dependent external quantum efficiency measurements are presented. This method allows us to estimate the optical and electronic losses in the solar cells, as well as estimate the effective band gap energy and its temperature dependence.

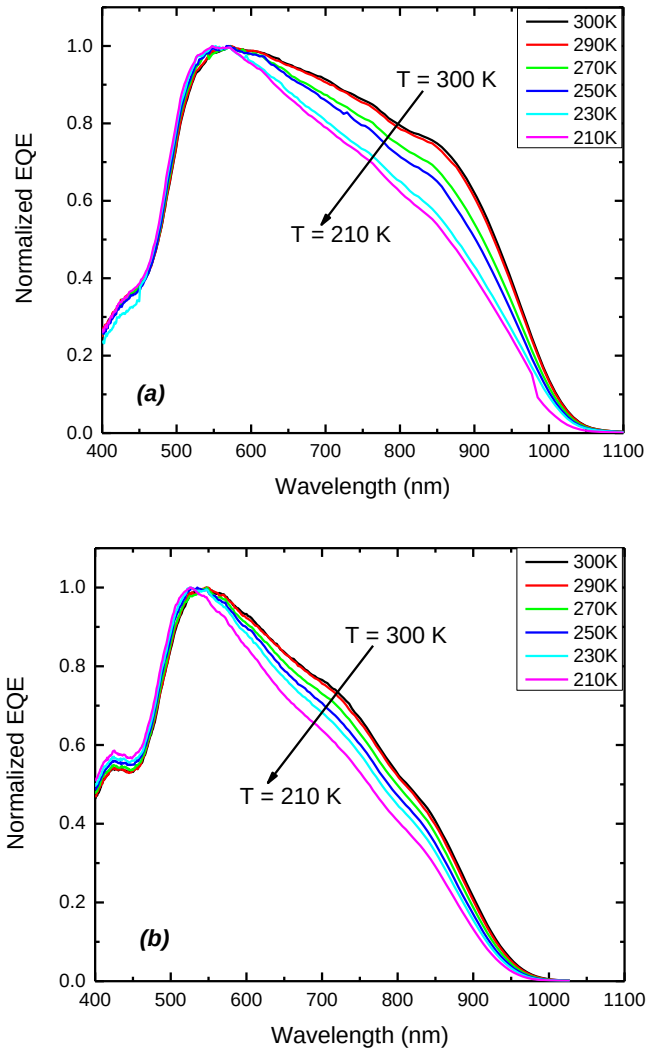

Figure 4.12: Normalized EQE curves obtained in the temperature range of 300K-210K. (a) – sample A, (b) – sample B.

Analyzing the EQE curves presented in figure 4.12 allows us to have a better understanding of the optical losses in the device: the drop in intensity in the 400-500nm region is due to the absorption of the CdS buffer layer, which has a band gap energy of 2.42 eV[22]; the big drop in intensity in the 540-1000nm region are recombinational losses.

These results obtained from EQE measurements are coinciding well with the results of IV measurements. For sample A, the squareness of the EQE curves indicates on better photocurrent collection in 540-1000nm region, which explains the higher current output, and the drop in photocurrent collection rate with lowering the temperature explains the rapid drop in FF. In the case of sample B, it can be seen from the "triangular" shape of EQE curves that in the same region there are huge recombinational losses, explaining the lower current output. However, the change in photocurrent collection in that region for sample B was not as high, which explains the low temperature-dependence of the FF obtained from IV measurements.

From the low energy region of the EQE curves – around 1.2-1.3 eV, the E_g^* effective band gap energy was estimated, by plotting $(E \times EQE)^2$ versus E. As can be seen on the figure (4.13-a), for both samples the trend is similar- with decreasing the temperature the effective band gap increases slightly. Using the obtained values for band gap energy, it is possible to estimate the V_{oc} deficiency, that is – the difference between the maximum V_{oc} that is theoretically achievable (based on Schockley-Quiesser limit) and the experimentally achieved value. References for ideal values for V_{oc} were taken from the paper of Russell M. Geisthardt[21].

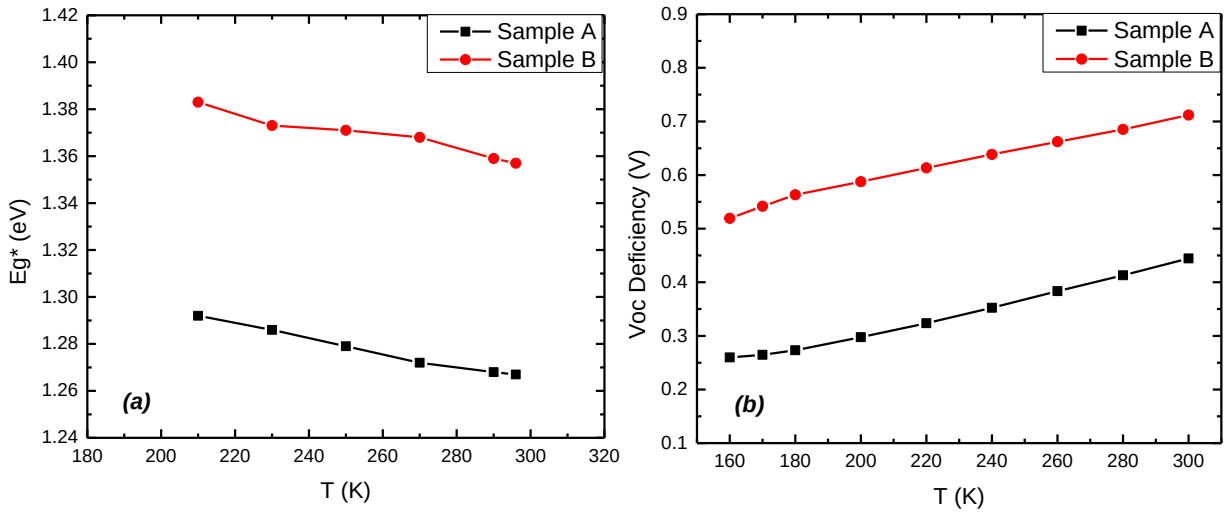

Figure 4.13: The temperature dependence of the E_g^* effective band gap energy (a) and V_{oc} deficiency (b) of the studied samples obtained from the EQE measurements.

Conclusions

From the temperature-dependent J-V measurements and analysis, the following conclusions were made:

- Sample B showed higher Fill Factor - around 45% compared to the 25% of sample A. It was also less temperature dependent, decreasing by a small amount regardless of illumination conditions (d(FF)/dT = ±0.03 %/K), while the sample A's FF was dropping significantly with lowering the temperature (d(FF)/dT = 0.06 %/K), and the drop was even more rapid for lower illumination intensities (d(FF)/dT = 0.1 %/K), which coincides with the high values of shunt conductance.
- Sample A had series resistance around 0.8 Ωcm^2 at room temperature and shunt resistance of around 0.66 $k\Omega cm^2$ and these values are lower than the suggested ones: around 1 $k\Omega cm^2$ for R_p, and 1 Ωcm^2 for R_s, indicating that there are significant parasitic losses. For sample A, the shunt resistance in the 200-250K region was decreasing with the decrease in temperature, which can be explained by the existence of the second diode in the solar cell structure. For sample B, series resistance was estimated to be 1 Ω/cm^2 at RT, and shunt resistance of 0.85 $k\Omega*cm^2$. For sample B, the parasitic resistances were closer to suggested values, and unlike sample A, the shunt resistance for sample B increases with a decrease in temperature, which should reduce the amount of parasitic losses.
- The dark saturation current of sample B is by orders of magnitude higher, which significantly limits the V_{oc}, resulting in almost twice as high V_{oc} deficiency of around 0.6V compared to 0.35V for sample A.
- The E_A activation energy of sample B was estimated to be 820 meV, which is lower compared to the 985 meV for sample A.
- Since there is a big difference between the band gap energy and the activation energy – around 300 meV for sample A and around 500 meV for sample B, we can conclude that the interface recombination predominates in both solar cells.

From the temperature-dependent EQE measurements and analysis, the conclusions are as follows:

- The effective band gap energy of sample B was estimated to be around 1.38 eV, which is much closer to the peak in the Shockley-Queisser limit (1.35eV), compared to the 1.27eV for sample A.
- From the shape of the EQE curves, it can be concluded, that there is a lot of bulk recombination in both devices, since the electron-hole pairs generated by photons of 600-900nm wavelength are lost due to a high recombination rate.

Summary

In this project, temperature-dependent current-voltage (J-V) characteristics and external quantum efficiency (EQE) of CCGSe-based MGL solar cells with differences in preparation were studied. The main aim of the work was to find the diode circuit parameters (ideality factor and dark saturation current) and parasitic loss parameters (series resistance and parallel resistance) from J-V curves and study their dependences on temperature and light intensity.

Main experiments were done in the temperature region of around 300K-200K, and the performance of the devices was analyzed in conditions with different illumination intensities, as well as in dark. From the analysis of the obtained experimental results, it was concluded, that the device with the nanoscale crystallization of the surface in the preparation process showed promising properties like improved band alignment and better parasitic resistances when comparing to the sample with the initial treatment. However, it had its own drawbacks: the limitation of the current output due to bigger recombinational current and the difference between the activation energy E_A and band gap energy E_g was even higher. Due to this big difference between E_A and E_g, it was concluded that in both devices interface recombination predominated.

At the same time from the EQE spectra, it was shown that due to large recombination rate of the electron-hole pairs generated by photons of 600-900nm wavelength, there is a lot of bulk recombination in the devices.

In conclusion, it can be said, that even though the sulfurization of the surface of the absorber layer has improved some properties, the process is not optimized yet, and it can be suggested to try the treatment with different thicknesses of the CdS layer.

References

[1] Miro Zeman, Delft University of Technology: Introduction to Photovoltaic Solar Energy

[2] American Association for the Advancement of Science: 4 Dec 2009 – staff report

[3] NASA Goddard Institute for Space Studies: A World of agreement – the temperatures are rising

[4] Mohammad Tawheed Kibria, Akil Ahammed, Saad Mahmud Sony, Faisal Hossain, Shams-Ul-Islam "A Review: Comparative studies on different generation solar cells technology" Institute of Energy, University of Dhaka, Dhaka-1000, Bangladesh

[5] M.Altosaar, A.Jagomagi, M.Kauk, M.Krunks, J.Krustok, E.Mellikov*, J.Raudoja, T.Varema, "Monograin layer solar cells": doi:10.1016/S0040-6090(03)00167-6

[6] Thin Solid Films 480-481 (2005) 307-311: doi: 10.1016/j.tsf.2004.11.006

[7] Wiliam D.Callister jr, "Fundamentals of materials science and engineering" 5th edition

[8] https://www.pveducation.org/pvcdrom/pn-junctions/types-of-recombination

[9] Dr. Alistair Sproul, The Key Centre for Photovoltaic Engineering, UNSW: Understanding the p-n Junction

[10] Andres Cuevas, *Research School of Engineering, The Australian National University, Canberra, ACT 0200, Australia:* "The recombination parameter J0", Energy Procedia 55 (2014) 53 – 62

[11] Thin film solar cells: Device measurements and analysis, Prog. Photovolt: Res. Appl. 2004; 12:155-176 (DOI: 10.1002/pip.518)

[12] https://www.pveducation.org/pvcdrom/welcome-to-pvcdrom/solar-cell-operation

[13] Energy Procedia 27 (2012) 135 – 142: Analysis of the Temperature Dependence of the Open-Circuit Voltage

[14] ISSN 2250-2459, ISO 9001:2008 Certified Journal, Volume 4, Issue 8, August 2014: Effect of Light intensity and Temperature on Crystalline Silicon Solar Modules Parameters

[15] Mati Danilson: Temperature Dependent Electrical Properties of Kesterite Monograin Solar Cells:2016

[16] https://www.solarinsure.com/largest-solar-power-plants

[17] Thin Solid Films 666 (2018) 15-19| https://doi.org/10.1016/j.tsf.2018.09.025

[18] Efficiency droop in gallium indium nitride (GaInN)/gallium nitride (GaN) LEDs

D.S. Meyaard, ... E.F. Schubert | Nitride Semiconductor Light-Emitting Diodes (LEDs): 2014

[19] Rapid and accurate determination of series resistance and fill factor losses in industrial silicon solar cells, S. Bowden and A. Rohatgi. School of Electrical and Computer Engineering, Georgia Institute of Technology, Atlanta GA 30332–0250 USA

[20] https://www.pveducation.org/pvcdrom/solar-cell-operation/quantum-efficiency

[21] Status and Potential of CdTe Solar-Cell Efficiency|DOI:10.1109/JPHOTOV.2015.2434594

[22] D. Lincot, Gary Hodes Chemical Solution Deposition of Semiconducting and Non-Metallic Films: Proceedings of the International Symposium The Electrochemical Society, 2006 ISBN 1-56677-433-0

[23] Nano-scale sulfurization of Cu 2 ZnSnSe 4 crystal surface for photovoltaic applications: DOI: 10.1039/C9TA08020A